CHEMISTRY OF MATERIALS

pubs.acs.org/cm Article

A Polar Magnetic and Insulating Double Corundum Oxide: Mn_2MnSbO_6 with Ordered Mn(II) and Mn(III) Ions

Hai L. Feng,[#] Chang-Jong Kang,[#] Bongjae Kim, Kyoo Kim, Mark Croft, Sizhan Liu, Trevor A. Tyson, Eli Stavitski, Rui Zu, Venkatraman Gopalan, Saul H. Lapidus, Corey E. Frank, Youguo Shi, David Walker, and Martha Greenblatt*

Cite This: *Chem. Mater.* 2021, 33, 6522−6529 Read Online

ACCESS | Metrics & More | Article Recommendations | Supporting Information

ABSTRACT: A new magnetic insulator Mn_2MnSbO_6 with a polar crystal structure and an ordered Mn^{2+} and Mn^{3+} arrangement was synthesized under a high pressure of 7.5 GPa and 1300 °C. The crystal structure of Mn_2MnSbO_6, investigated by synchrotron powder X-ray diffraction, was found to be isomorphous with that of Ni_3TeO_6-type, space group *R*3. The non-centrosymmetric structure was confirmed by the second-harmonic generation measurements. The X-ray absorption near-edge spectroscopy measurement confirmed the nominal oxidation states of $Mn^{2+}{}_2Mn^{3+}SbO_6$. Magnetic measurements indicate that Mn_2MnSbO_6 orders antiferromagnetically below 44 K and undergoes a field-induced spin-flop transition at 5 K. First-principles calculations indicate an antiferromagnetic ground state with up/up/up/down/down/down (uuuddd) spin configuration of the six crystallographically unique Mn ions in the *c*-axis doubled magnetic structure. The density functional theory calculations also substantiate the experimentally observed charge ordering of the Mn^{2+}/Mn^{3+} ions and the insulating behavior due to a bandgap of 0.52 eV. To the best of our knowledge, this is the first double corundum oxide containing Jahn−Teller active Mn^{3+} ions.

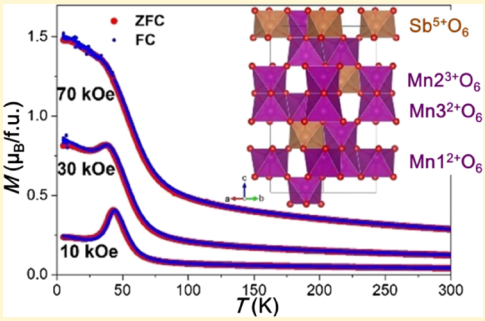

■ INTRODUCTION

Materials exhibiting both ferromagnetic or antiferromagnetic (FM or AFM) and ferroelectric (FE) ordering are rare and are desired for their promising application in future electronic devices.[1] So far, most of the reported multiferroic compounds are oxides, and one of the important directions to search for new multiferroic materials is to synthesize oxides with magnetic ordering and non-centrosymmetric structures.[2,3] Recently, double corundum oxides, with the general formula $A_2BB'O_6$, usually crystallizing in Ni_3TeO_6- or $LiNbO_3$-type non-centrosymmetric crystal structures,[4] have been attracting great attention because the magnetoelectric effect has been reported in corundum oxides Mn_3WO_6, Co_3TeO_6, and Ni_3TeO_6.[5−12] So far, the number of reported double corundum oxides is limited,[4] presumably because most of them require high synthesis pressure (5 GPa or higher) to stabilize the structure type with relatively small A site ions, such as Mn^{2+} and Ni^{2+}. Most of the reported double corundum oxides have Mn^{2+} ions in the A sites, for instance, $Mn_2BB'O_6$ (B = Mn, Fe, Sc, or In; B' = W, Sb, Nb, Ta, or Mo).[5,13−19] For Mn_3WO_6 and Mn_3TeO_6, the B sites are also occupied by Mn^{2+} ions. However, to the best of our knowledge, there is no reported double corundum oxide containing Mn^{3+} ions. It is well established that oxides with $Mn^{3+}O_6$ octahedra tend to display Jahn−Teller distortions and can drive interesting magnetic behaviors.[20−24] In this work, we aimed to introduce the Mn^{3+} ion to the B-site of double corundum oxide by substituting hexavalent W^{6+}/Te^{6+} with pentavalent Sb^{5+}. Using high-pressure methods, we successfully synthesized a new double corundum oxide Mn_3SbO_6 ($Mn^{2+}{}_2Mn^{3+}SbO_6$) with both Mn^{2+} and Mn^{3+} ions in an ordered arrangement. In this paper, we report the results of crystal structure determined by synchrotron powder X-ray diffraction, X-ray absorption near-edge spectroscopy (XANES), studies of the temperature-dependent magnetic susceptibility, and the magnetic and electronic band structure as determined by first-principles calculations.

■ EXPERIMENTAL SECTION

Synthesis. A polycrystalline sample of Mn_2MnSbO_6 was synthesized under high-pressure and high-temperature conditions. Powders of MnO (99.9%, Alfa), Mn_2O_3 (99.9985%, Alfa), and Sb_2O_5 (99.99%, Alfa), with a molar ratio 2:0.5:0.5, were weighted and ground well. The ground powder was then sealed in Pt capsules, which were put inside MgO crucibles. The crucibles were then

Received: June 15, 2021
Revised: July 28, 2021
Published: August 11, 2021

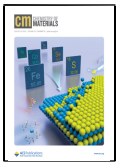

https://doi.org/10.1021/acs.chemmater.1c02046
Chem. Mater. 2021, 33, 6522−6529

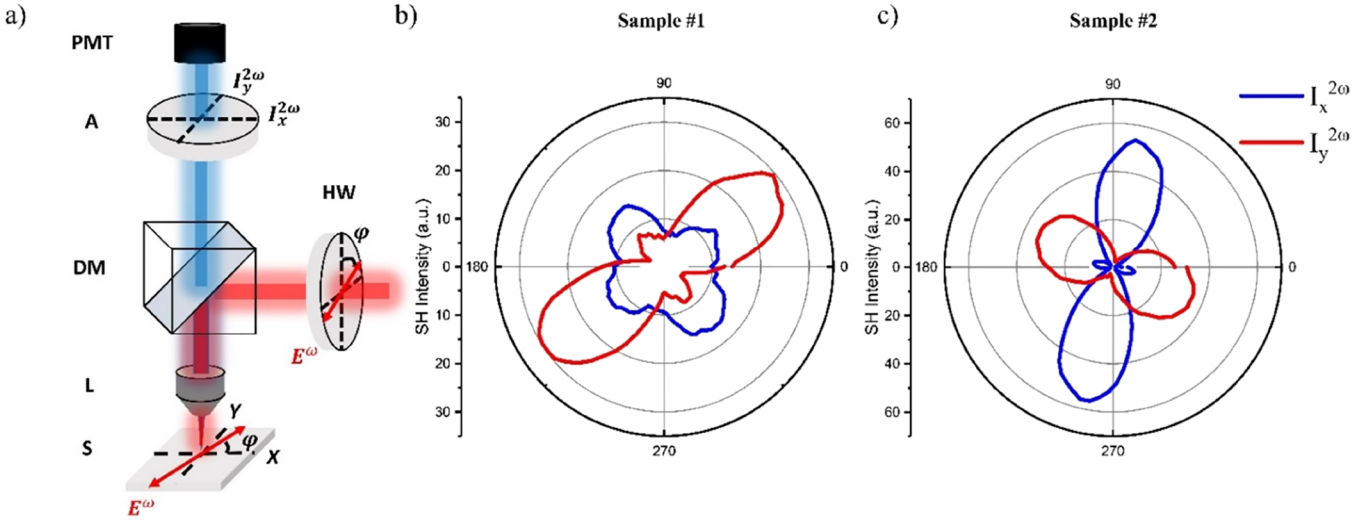

Figure 1. Schematic of SHG measurement and second-harmonic intensity of Mn_2MnSbO_6 versus the polarization direction (φ) of the incident beam. (a) Schematic of SHG setup. HW, S, L, DM, A, and PMT represent half waveplate, sample, lens, dichroic mirror, analyzer, and photomultiplier tube, respectively. The red and blue rays correspond to fundamental (800 nm) and second-harmonic (400 nm) waves, respectively. E^{ω}, $I_x^{2\omega}$, and $I_y^{2\omega}$ are incident electric field and the SH intensity polarized along the X and Y directions, respectively. (b,c) SHG polar plots as a function of φ for two independent samples. The blue and red curves correspond to $I_x^{2\omega}$ and $I_y^{2\omega}$, respectively.

statically compressed using a Walker-type multianvil press[25] at a pressure of 7.5 GPa, followed by heating at 1300 °C for 2 h, at the high pressure. The sample was then quenched to ambient temperature before the pressure was released (sample number: GG1393).

Second-Harmonic Generation Measurement. Second-harmonic generation (SHG) measurements have been widely used to confirm non-centrosymmetry in materials.[26−30] The SHG measurements were carried out at room temperature in normal reflection mode on polished samples. SHG measurement is an all-optical technique where two photons of frequency ω with fields E_j and E_k and polarization directions j and k interact with a material with a nonzero d_{ijk} tensor (non-centrosymmetric) and generate polarization $P_i^{2\omega}$ of frequency 2ω in the i direction. The SHG intensity, $I^{2\omega}$, was detected with a Hamamatsu photomultiplier tube. A Ti-sapphire laser (Spectra-Physics) with an output of 800 nm, 80 fs pulses at 1 kHz frequency was used.

Synchrotron Powder X-Ray Diffraction. Parts of the as-synthesized samples were ground to a fine powder, which was characterized by synchrotron powder X-ray diffraction (SPXD, λ = 0.45788 Å) at ambient temperature at Beamline 11-BM of the Advanced Photon Source of Argonne National Laboratory. Rietveld refinements of the powder diffraction data were carried out with the RIETAN-software,[31] and the crystal structures were drawn with VESTA.[32]

X-Ray Absorption Near-Edge Spectroscopy. Mn−K edge XANES data were collected in both the transmission and fluorescence modes with simultaneous standards. All the spectra were fit to pre- and post-edge backgrounds and normalized to unity absorption edge step across the edge.[13,33−36] The XANES spectra of the title compound were collected at the ISS 8ID with a Si(111) double crystal monochromator. The standard spectra[13,33−36] were collected at the QAS, 7BM Beamline at NSLS-II; and at beamline X-19A at NSLS-I with a Si-111 double crystal monochromator.

Magnetic Measurements. The temperature dependence of magnetization was measured using a vibrating sample magnetometer (VSM-7 T, Quantum design). The measurements were taken under zero-field-cooled and field-cooled conditions in the temperature range 2−300 K and in the applied magnetic fields of 10, 30, and 70 kOe. Isothermal magnetization curves were recorded between magnetic fields of ±70 kOe at temperatures of 5 and 100 K with the same VSM. The temperature dependence of the specific heat (Cp) was measured on a physical properties measurement system (PPMS-14 T, Quantum Design) using the HC option (relaxation method).

Density Functional Theory Calculations. The all-electron full-potential linearized augmented plane-wave method implemented in WIEN2k[37] was adopted to determine the electronic structure. Structural parameters were taken from SPXD refinements. Generalized gradient approximation (GGA) of Perdew−Burke−Ernzerhof (PBE)[38] was chosen for the exchange-correlation functional. A 17 × 17 × 17 k-mesh was used for the Brillouin zone integration. The muffin tin radii were chosen to be 1.98, 2.11, and 1.70 Bohr for Mn, Sb, and O, respectively, and the size of a plane-wave basis set was determined from $R_{mt}K_{max}$ of 7.0, where R_{mt} is the smallest atomic muffin tin radius and K_{max} is the largest plane-wave vector. The spin-orbit coupling (SOC) makes Mn 3d orbital a more atomic-like state and helps to obtain an insulating phase of the system, which was included in the second-variational scheme. To consider the strong correlation effect, GGA + U was adopted within fully localized limit.[39,40] The effective on-site Coulomb interaction parameter $U_{eff} = U - J = 6$ eV was used.

■ RESULTS AND DISCUSSION

SHG Polarimetry. According to the equation $P_i = d_{ijk}E_jE_k$ in Einstein Notation,[26] SHG depends on the third rank tensor d_{ijk}, which will only exist in non-centrosymmetric point groups. Thus, only materials with non-centrosymmetric point groups will exhibit dipolar SHG signals. The SHG was measured in the normal reflection geometry at room temperature by rotating the polarization direction of the fundamental beam at 800 nm (depicted as φ) so that SHG (400 nm) is detected by the photomultiplier tube (PMT) along two orthogonal Lab X-axis and Y-axis, which are shown as the blue and red plots in Figure 1, respectively. The SHG response shows dependence on the polarization direction of the incident beam, confirming that Mn_2MnSbO_6 is SHG-active. The SHG polar plots can typically be fitted to extrapolate the point group symmetry, orientations, and relations between SHG coefficients. Due to the polycrystalline nature of the crystals, it is not useful to fit the polarimetry data in this work.

Crystal Structure. The room-temperature SPXD pattern of Mn_2MnSbO_6 can be well indexed with a hexagonal cell of a = 5.26 Å and c = 14.26 Å. Comparable unit cells have been reported for similar double corundum oxides Mn_2FeMO_6 (M

https://doi.org/10.1021/acs.chemmater.1c02046
Chem. Mater. 2021, 33, 6522−6529

= Nb, Ta),[14] Mn_2ScMO_6 (M = Nb, Ta, Sb),[15,18] Mn_2MWO_6 (M = Fe, Mn),[5,13] and Mn_2FeSbO_6.[17] Space groups *R*3*c*, *R*3, and *R*-3*c* are reported for these oxides. The centrosymmetric *R*-3*c* can be excluded because Mn_2MnSbO_6 is confirmed from SHG analysis to crystallize in a non-centrosymmetric space group. Refinements of the SPXD pattern with *R*3*c* and *R*3 space groups found that the pattern can be well refined with space group *R*3 (see Figure 2). When refined with *R*3*c*, the

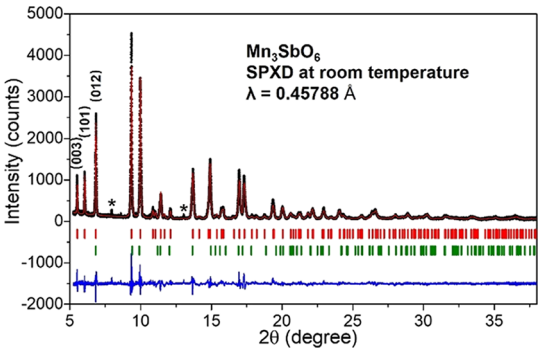

Figure 2. Rietveld analysis of SPXD patterns for Mn_2MnSbO_6. The experimental and theoretical data are shown as black and red patterns, respectively. The blue pattern indicates their difference. The vertical bars represent the Bragg reflections for the Mn_2MnSbO_6 (red) and the impurity phase $Mn_4Sb_2O_9$ (green), respectively. The estimated content for the impurity phase $Mn_4Sb_2O_9$ is 4.9 wt %. The asterisks mark the strongest peaks of unidentified impurities.

low-angle peaks, (003) and (101), could not be well fitted (see the Supporting Information). In space group *R*3, there are four distinguishable sites, 6*c* (0, 0, *z*), to accommodate Mn1, Mn2, Mn3, and Sb ions, which is isostructural to the Ni_3TeO_6-type crystal structure. The refined cell parameters, atomic positions, and displacement factors are summarized in Table 1.

Table 1. Refined Atomic Positions and Displacement Factors of Mn_2MnSbO_6[a]

atom	Wyckoff site	*x*	*Y*	*z*	B_{iso} (Å^2)
Mn1	3*a*	0	0	0.2120(9)	0.58(1)
Mn2	3*a*	0	0	0.6956(9)	0.58(1)
Mn3	3*a*	0	0	0.4888(9)	0.58(1)
Sb	3*a*	0	0	−0.0007(9)	0.58(1)
O1	9*b*	−0.0253(19)	0.2940(13)	0.0927[b]	1.92(7)
O2	9*b*	0.009(3)	0.7141(17)	0.5963[b]	1.92(7)

[a]Space group: *R*3 (no. 146). Cell parameters: *A* = 5.26163(7) Å, *c* = 14.26480(7) Å, *V* = 342.009(9) Å^3, *Z* = 3, and d_{cal} = 5.57 g/cm^3. *R* values: R_{wp} = 12.49%, R_p = 9.8%, and *S* = 1.61. In the final refinement, the B_{iso} parameters for Mn1, Mn2, Mn3, and Sb are constrained to be equal, while the B_{iso} parameters for O1, and O2 were also constrained to be equal. [b]These values were refined separately during the refinement but fixed at the final refinement.

The refined crystal structure of Mn_2MnSbO_6 is displayed in Figure 3. Mn_2MnSbO_6 consists of $Mn2Mn3O_9$ ($Mn1SbO_9$) dimer units formed by face-sharing $Mn2O_6$($Mn3O_6$) and $Mn1O_6$(SbO_6) octahedra. The enlarged $Mn2Mn3O_9$ and $Mn1SbO_9$ dimer units are displayed on the right side of Figure 3. Within each dimers, the Mn ions deviate from the center of the octahedra and are far apart, resulting in three shorter Mn−O bonds and three longer Mn−O bonds for each MnO_6 octahedra, which is possibly due to the electrostatic

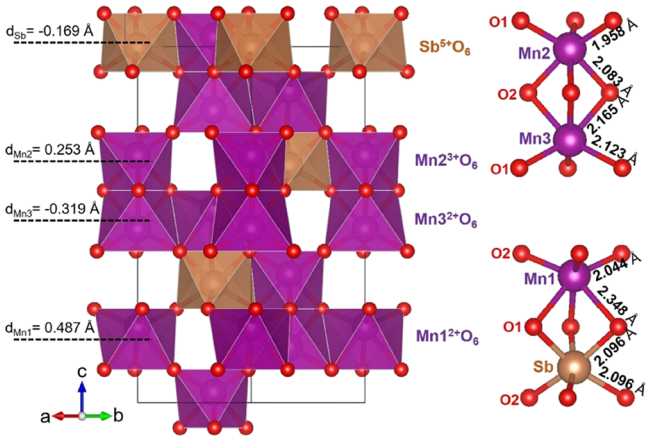

Figure 3. Crystal structure of Mn_2MnSbO_6 refined from room-temperature SPXD data. The enlarged $Mn2Mn3O_9$ and $Mn1SbO_9$ dimer units are shown on the right side; also indicated on the left is the magnitude of displacement of the Mn and Sb ions from the center of their respective octahedra.

repulsion between cations within the dimer. The displacements from the center of octahedra for each cation are displayed in Figure 3. The detailed bond lengths are summarized in the Supporting Information. Bond valence sum calculated from the bond lengths are +2.17, +3.01, and + 2.13 for Mn1, Mn2, and Mn3, respectively. This indicates that the Mn1 and Mn3 sites are mainly Mn^{2+} and the Mn2 site is mainly Mn^{3+}; thus the Mn^{2+} and Mn^{3+} ions are arranged in an ordered manner. Note that the average bond length between Mn and O atoms in $Mn^{3+}O_6$ octahedra (∼2.0 Å) is shorter than that in $Mn^{2+}O_6$ (∼2.2 Å). The $Mn^{3+}O_6$ octahedra in corundum oxide Mn_2MnSbO_6 does not show typical Jahn−Teller distortion observed in other Mn^{3+} perovskite oxides.[20−24] The valence state of Mn ions is further studied by XANES. Because the cations are off the center along the *c*-axis in Mn_2MnSbO_6, a theoretical value of polarization along the *c*-axis could be calculated from the charges, *q*, and their displacement along the *c*-axis, d^c, according to the equation $P = \left(\sum_j q_j d_j^c\right)/V$, where *V* is the volume of the unit cell. In this calculation, the Mn1 and Mn3 cations are assumed to be 2+ and the Mn2 cations are assumed to be 3+. The calculated polarization is about 3.5 μC cm^{-2}, which is comparable with the value of 4.0 μC cm^{-2} calculated for a similar double corundum oxide Mn_2ScTaO_6.[18]

Mn-K XANES. XANES measurements of the K-edges of 3d row transition metals in compounds have proven to be a useful probe of the transition metal valence/configuration.[13,33−36] These edges are dominated by peak-like 1s to 4p transitions and typically exhibit a chemical shift to higher energies with increasing transition metal valance. Here the chemical down-shift in energy, with decreasing valence, can be monitored by either the energy of the peak or the rapidly rising portion of the near-edge spectra. Referring to Figure 4, the chemical down-shift of the peak-energy between the perovskite-based (with corner-sharing O-octahedra) $CaMn^{4+}O_3$, $LaMn^{3+}O_3$, and $LaSrMn^{2+}SbO_6$ standards is quite clear.[33,34] A splitting of the edge features in the NaCl structure (with edge-sharing O-octahedra) $Mn^{2+}O$ spectrum should be noted.[36]

The Mn−K main edges of the Ni_3TeO_6-type structure Mn_2MnSbO_6 and the $Mn^{2+}{}_2FeWO_6$ compounds are also shown in Figure 4. Importantly the spectral peak of the

https://doi.org/10.1021/acs.chemmater.1c02046
Chem. Mater. 2021, 33, 6522−6529

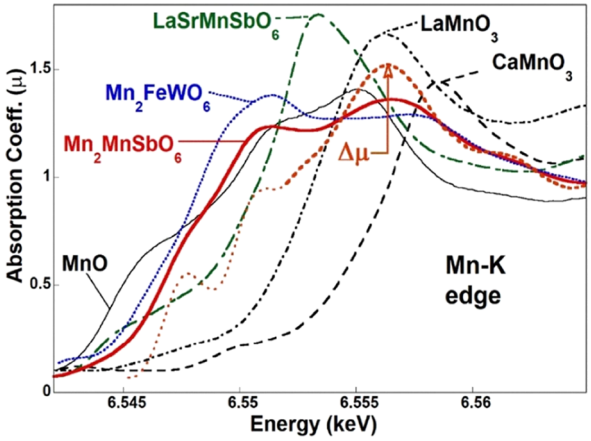

Figure 4. (a) Mn−K main-edge of Mn_2MnSbO_6 is compared to the edges of a series of standard compounds with differing formal valence states and local structure. The octahedrally coordinated standard spectra are $Mn^{2+}O$ (NaCl structure with edge-sharing) and the B-site (corner-sharing) perovskite-based $CaMn^{4+}O_3$, $LaMn^{3+}O_3$, and $LaSrMn^{2+}SbO_6$. The Ni_3TeO_6-type structure $Mn^{2+}{}_2FeWO_6$ standard is also shown. The difference spectrum $\Delta\mu = 3\,[\mu(Mn_2MnSbO_6) - \mu(Mn^{2+}{}_2FeWO_6)\ 2/3]$ assumes a $Mn^{2+}{}_2Mn^{3+}SbO_6$ valence distribution and subtracts a weighted $\mu(Mn^{2+}{}_2FeWO_6)$ spectrum (with renormalization) to have $\Delta\mu$ approximate/highlight the Mn^{3+} contribution in $Mn_2Mn^{3+}SbO_6$. Note that the heavy-dashed curve of $\Delta\mu$ highlights the Mn^{3+} contribution and the $\Delta\mu$ curve at lower energies is shown as weak-dashed points.

$Mn^{2+}{}_2FeWO_6$ spectrum is shifted well down in energy from the perovskite-Mn^{2+} standard, as is typical of Ni_3TeO_6 structure compounds.[13,18] The Mn_2MnSbO_6 spectrum manifests a prominent/similar local peak feature in the same energy range, strongly suggesting a $Mn^{2+}{}_2$ component in the compound formula. However, the absolute peak of the Mn_2MnSbO_6 spectrum occurs at an energy characteristic of a Mn^{3+} peak feature (i.e., compared to $LaMn^{3+}O_3$ in the figure). Thus, these dual features suggest $Mn^{2+}{}_2Mn^{3+}SbO_6$ assignment for this compound. In order to emphasize the underlying Mn^{3+} component feature, a normalized difference spectrum $\Delta\mu = 3[\mu(Mn_2MnSbO_6) - \mu(Mn^{2+}{}_2FeWO_6)\ 2/3]$ was calculated to approximately remove the $Mn^{2+}{}_2$ spectral contribution thereby highlighting the important Mn^{3+} component. As is clear in Figure 4, $\Delta\mu$ exhibits an extremely prominent peak at precisely the same energy as the $LaMn^{3+}O_3$ peak feature. The structure in the $\Delta\mu$ spectrum at lower energies is indicated by weak-dashed points do indeed represent extra spectral features in the Mn_2MnSbO_6 spectrum but are beyond the intended scope of this discussion emphasizing the Mn^{3+} component in the spectrum.

Magnetism. The resistance of Mn_2MnSbO_6 was out of range when measured at room temperature with a multimeter (maximum 200 MΩ); thus Mn_2MnSbO_6 is electrically insulating. The temperature dependence of magnetic susceptibility, $\chi(T)$, of Mn_2MnSbO_6 measured at 10, 30, and 70 kOe is shown in Figure 5a. The $\chi(T)$ value measured at 10 kOe displays a sharp peak at 44 K and indicates a possible antiferromagnetic (AFM) order, which is supported by the temperature dependence of specific heat, $C_p(T)$, with a λ-type anomaly at the corresponding temperature (T_N = 44 K). When $\chi(T)$ is measured at a higher magnetic field of 30 kOe, the peak becomes less prominent. The peak disappeared when $\chi(T)$ was measured at 70 kOe, which indicated that a possible field-induced magnetic transition occurred and suppressed the AFM state.

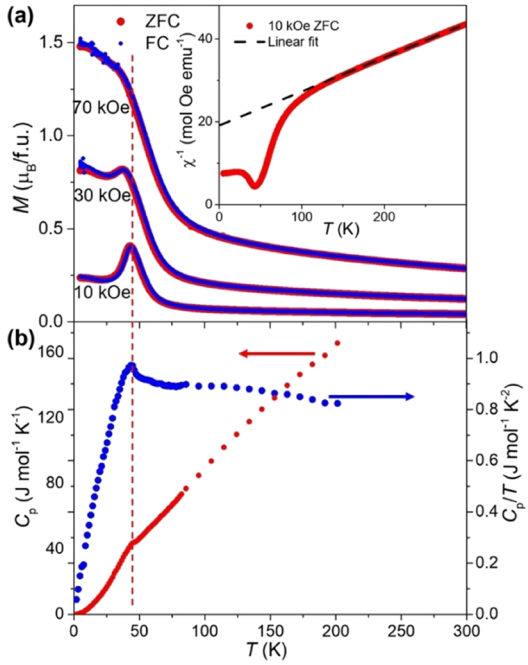

Figure 5. (a) Temperature dependence of magnetic susceptibility, $\chi(T)$, of Mn_3SbO_6 measured at 10, 30, and 70 kOe. The inset shows the corresponding $\chi^{-1}(T)$ curve measured at 10 kOe. (b) Temperature dependence of specific heat curves, $C_p(T)$ (left axis), and their corresponding $C_p/T(T)$ curves (right axis) of Mn_3SbO_6.

The $\chi^{-1}(T)$ curve, displayed in the inset of Figure 5a, shows Curie−Weiss (CW) behavior in the high-temperature region (150−300 K), but clearly deviates from CW behavior at temperatures lower than ∼100 K. Fitting the 150−300 K χ data with the CW law resulted in a Weiss temperature (θ_W) of −232 K and an effective moment of 9.88 μ_B. The large negative θ_W indicates that AFM interactions are dominant in Mn_2MnSbO_6, which is consistent with the observed AFM order at 44 K. The obtained μ_{eff} of 9.88 μ_B is close to the calculated spin-only moment of 9.70 μ_B for two Mn^{2+} (S = 5/2) ions and one Mn^{3+} (S = 2) ion, in agreement with our expected oxidation states for the Mn ions. The frustration factor, $|\theta_W/T_N|$ = 5.3, indicates a moderate frustration in the Mn_2MnSbO_6.

To further understand the magnetic order, the isothermal magnetization curves, M(H), measured at 100 and 5 K are shown in Figure 6. The M(H) data show linear correlation at

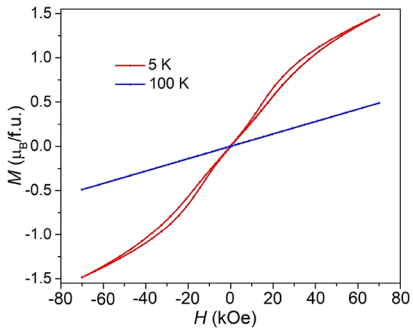

Figure 6. Isothermal magnetization curves of Mn_3SbO_6.

https://doi.org/10.1021/acs.chemmater.1c02046
Chem. Mater. 2021, 33, 6522−6529

100 K above the magnetic order temperature, which is consistent with the expected paramagnetic state. At 5 K, the M(H) curve shows linear behavior and no hysteresis when the magnetic fields are less than 10 kOe, supporting the AFM ground state. When the magnetic fields further increase to 70 kOe, the M(H) curves deviate from linear behavior and show a hysteresis loop between 10 and 70 kOe, indicating a possible field-induced spin-flop transition, which is also supported by the $\chi(T)$ curves measured at varied magnetic fields. At 5 K and 70 kOe, the magnetization is still not saturated, and the magnetization of 1.49 μ_B/f.u. is much smaller than the expected value of 14 μ_B/f.u., if all the Mn^{2+} and Mn^{3+} ions were FM-coupled in Mn_2MnSbO_6; these observations suggest that Mn_2MnSbO_6 is in a ferrimagnetic state at 5 K and 70 kOe, and a much stronger magnetic field is required to induce an FM state in Mn_2MnSbO_6.

Density Functional Theory Calculations. Density functional theory (DFT) calculations were carried out to explore the magnetic ground state of Mn_2MnSbO_6 and to study the corresponding electronic structure. Since the magnetic susceptibility measurement (Figure 5) indicates an AFM order, the unit-cell described in Table 1 should be doubled along the *c*-axis to allow an AFM order in the structure of Mn_2MnSbO_6. Note that a similar compound, Ni_3TeO_6, has a collinear AFM structure with a doubled unit cell along the *c*-axis.[41] There are 12 symmetrically different AFM orders available in the doubled unit cell. First, the total energies as a function of the on-site Coulomb interaction parameter, *U*, were calculated for the FM and all the possible AFM-ordered structures, which are shown in Figure 7. Here, the collinear AFM orders were only considered in the DFT calculations. There is a possibility of noncollinear AFM order for the double corundum system (e.g., Mn_2MnWO_6 was reported to have a noncollinear AFM structure[5]), which may change the details of the electronic structure, but does not alter the general conclusion of our study.

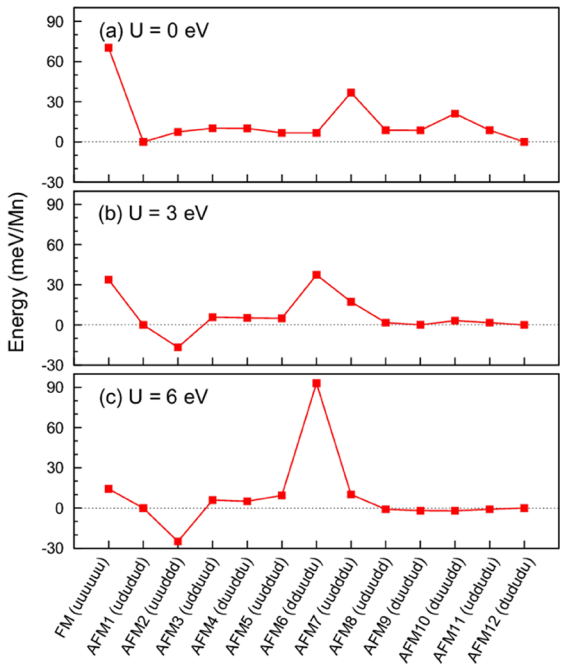

Figure 7. Total energies for FM and possible AFM orders of Mn_2MnSbO_6 computed using the GGA + SOC + *U* method. The unit of the total energy is meV/Mn. (a) *U* = 0 eV, (b) *U* = 3 eV, and (c) *U* = 6 eV. For each *U* value, the total energy of the AFM1 (ududud) order is chosen for reference.

As shown in Figure 7, the AFM1 (ududud) order is the magnetic ground state of Mn_2MnSbO_6 for *U* = 0 eV, while the AFM2 (uuuddd) order has the lowest energy for *U* = 3 and 6 eV. Figure 8 shows the two possible representative AFM orders in Mn_2MnSbO_6: AFM1 and AFM2. The AFM1 order corresponds to the collinear AFM approximation of the noncollinear AFM structure observed experimentally in a similar compound of Mn_2MnWO_6,[5] where spin moments of Mn1, Mn2, Mn3, Mn4, Mn5, and Mn6 are ordered in up, down, up, down, up, and down manner, respectively, that is, (ududud) order, for simple notation. Manganese oxide is a well-known strongly correlated system and requires a significant on-site Coulomb repulsion *U* in DFT calculations,[42] so Mn_2MnSbO_6 requires a sizable *U* as well and its magnetic ground state is more likely to be AFM2. The spin moments are ordered in the (uuuddd) manner for the AFM2 order of Mn_2MnSbO_6. It is noteworthy that the double corundum Ni_3TeO_6 has also the same AFM2 magnetic structure[41] as Mn_2MnSbO_6, while a similar corundum oxide Mn_2MnWO_6 has a noncollinear magnetic structure approximate to the AFM1 (ududud) order.[5] The two different AFM orders realized in two similar compounds, Mn_2MnSbO_6 and Mn_2MnWO_6, may originate from the fact that W^{6+} ($5d^0$)

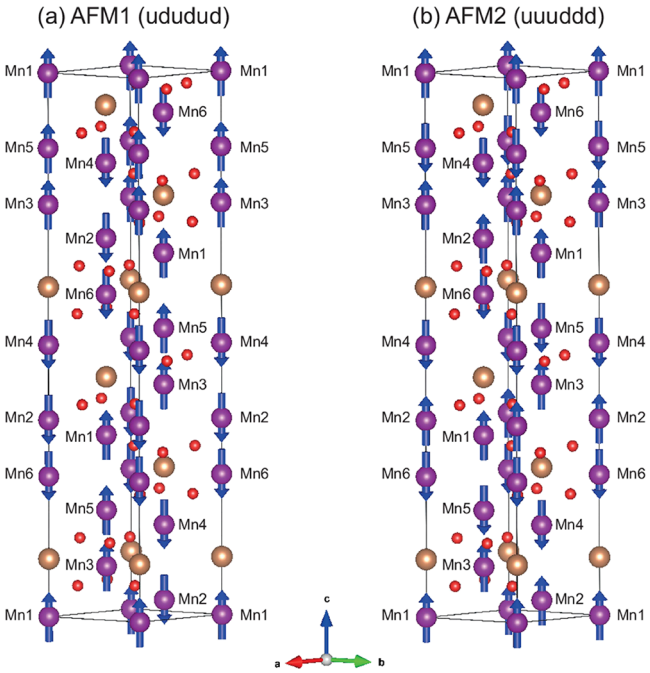

Figure 8. Two possible representative AFM orders in Mn_2MnSbO_6. Violet, orange, and red-colored spheres correspond to Mn, Sb, and O atoms, respectively. The unit cell is doubled along the *c*-axis. Six symmetrically different Mn atoms are presented in the AFM magnetic structures. (a) AFM1 order. Spin moments of Mn1, Mn2, Mn3, Mn4, Mn5, and Mn6 are ordered in an up, down, up, down, up, and down manner, respectively, which is referred to as the (ududud) order. It corresponds to the collinear AFM approximation of the noncollinear AFM order observed in Mn_2MnWO_6.[5] (b) AFM2 order. Spin moments of Mn1, Mn2, Mn3, Mn4, Mn5, and Mn6 are ordered in an up, up, up, down, down, and down manner, respectively, referred to as the (uuuddd) order.

https://doi.org/10.1021/acs.chemmater.1c02046
Chem. Mater. 2021, 33, 6522−6529

and Sb^{5+} ($5d^{10}$) have different electronic configurations, which could have a large influence on the superexchange interactions through these ions.[43,44] Moreover, Mn_2MnSbO_6 has two Mn^{2+} and one Mn^{3+} magnetic ions, while Mn_2MnWO_6 has three Mn^{2+} magnetic ions. The different magnetic ions would also contribute to the different magnetic interactions, resulting in the different AFM orders.

Figure 9 shows the total and partial density of states (DOS) of Mn_2MnSbO_6 for the magnetic ground state of the AFM2 (uuuddd) order. It is noteworthy that without the on-site Coulomb interaction parameter U, Mn_2MnSbO_6 remains metallic regardless of any of the magnetic structures, whereas for U = 6 eV, it becomes insulating for all the magnetic structures except for AFM6, which has a significant total energy compared to the others (Figure 7). The size of a gap opening in the AFM2 magnetic structure is 0.52 eV at U = 6 eV. Thus, the on-site Coulomb interaction parameter U is necessary for obtaining the insulating state, as well as the correct magnetic ground-state structure. It validates the theoretical AFM2 magnetic structure as the ground state for Mn_2MnSbO_6. Moreover, as shown in the partial DOS in Figure 9, the spin majorities of Mn1, Mn2, Mn4, and Mn5 are fully occupied, while those of Mn3 and Mn6 are not, consistent with the effective oxidation state of Mn1, Mn2, Mn4, and Mn5 as Mn^{2+} and corresponding electronic configuration of d^5, whereas Mn3 and Mn6 as Mn^{3+} with d^4 configuration. This charge ordering, established by the structural analysis of Mn_2MnSbO_6 above, is corroborated by the ordered spin magnetic moments at the Mn sites as well. The spin magnetic moments are 4.39, 4.39, 3.76, −4.39, −4.39, and − 3.76 μ_B, respectively, for Mn1, Mn2, Mn3, Mn4, Mn5, and Mn6 ions, where the minus sign indicates the opposite direction of the first three spin magnetic moments. Deviations from integer values of 5 and 4 in the spin magnetic moments of Mn^{2+} and Mn^{3+} sites are due to the large hybridization between Mn 3d and O 2p orbitals as demonstrated in Figure 9.

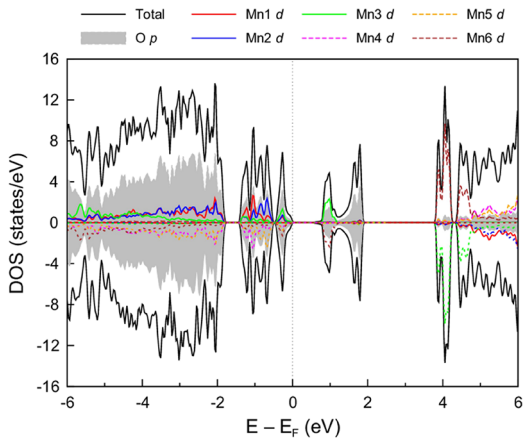

Figure 9. Total and partial density of states (DOS) of Mn_2MnSbO_6 for the magnetic ground state of AFM2 (uuuddd) order from GGA + SOC + U (= 6 eV) calculation. Black solid line corresponds to the total DOS. The positive and negative values in DOS correspond to spin up and down, respectively.

■ CONCLUSIONS

A new double corundum oxide Mn_2MnSbO_6 was successfully synthesized under high-pressure conditions of 7.5 GPa and 1300 °C. The crystal structure of Mn_2MnSbO_6, investigated by SPXD, was found to crystallize in the Ni_3TeO_6-type crystal structure with the space group $R3$. The Mn^{2+} and Mn^{3+} ions are arranged in an ordered manner. Mn_2MnSbO_6 was confirmed to be non-centrosymmetric by SHG analysis. The XANES measurements confirms the nominal oxidation states of $Mn^{2+}{}_2Mn^{3+}SbO_6$. Magnetic measurements indicate that Mn_2MnSbO_6 orders antiferromagnetically below 44 K and undergoes a field-induced spin-flop transition at 5 K. Thus, a new magnetic insulator, Mn_2MnSbO_6 with a polar crystal structure and ordered Mn^{2+} and Mn^{3+} arrangement was synthesized. First-principles calculations find an antiferromagnetic ground state with an up, up, up, down, down, down (uuuddd) spin configuration of the six unique Mn ions in the c-axis doubled magnetic structure. This (uuuddd) magnetic spin order opens a 0.52 eV bandgap in the DOS consistent with the experimentally observed insulating behavior of Mn_2MnSbO_6. The DFT calculations also confirm the experimentally observed charge ordering of the Mn^{2+}/Mn^{3+} ions. To the best of our knowledge, this is the first double corundum oxide with Jahn−Teller active Mn^{3+} ions.

■ ASSOCIATED CONTENT

Supporting Information

The Supporting Information is available free of charge at https://pubs.acs.org/doi/10.1021/acs.chemmater.1c02046.

Rietveld analysis of SPXD patterns of Mn_2MnSbO_6 with space group $R3c$ (Figure S1); Selected bond lengths of Mn_2MnSbO_6 (Table S1) (PDF)

■ AUTHOR INFORMATION

Corresponding Author

Martha Greenblatt − *Department of Chemistry and Chemical Biology, Rutgers, The State University of New Jersey, Piscataway, New Jersey 08854, United States;* orcid.org/0000-0002-1806-2766; Email: greenbla@chem.rutgers.edu

Authors

Hai L. Feng − *Department of Chemistry and Chemical Biology, Rutgers, The State University of New Jersey, Piscataway, New Jersey 08854, United States; Beijing National Laboratory for Condensed Matter Physics, and Institute of Physics, Chinese Academy of Sciences, Beijing 100190, China;* orcid.org/0000-0002-2699-3958

Chang-Jong Kang − *Department of Physics, Chungnam National University, Daejeon 34134, South Korea;* orcid.org/0000-0003-2895-4888

Bongjae Kim − *Department of Physics, Kunsan National University, Gunsan 54150, South Korea;* orcid.org/0000-0002-3841-2989

Kyoo Kim − *Korea Atomic Energy Research Institute (KAERI), Daejeon 34057, South Korea*

Mark Croft − *Department of Physics and Astronomy, Rutgers, The State University of New Jersey, Piscataway, New Jersey 08854, United States*

Sizhan Liu − *Department of Physics, New Jersey Institute of Technology, Newark, New Jersey 07102, United States*

Trevor A. Tyson − *Department of Physics, New Jersey Institute of Technology, Newark, New Jersey 07102, United States;* orcid.org/0000-0001-6587-9296

https://doi.org/10.1021/acs.chemmater.1c02046
Chem. Mater. 2021, 33, 6522−6529

Eli Stavitski − *National Synchrotron Light Source II, Brookhaven National Laboratory, Upton, New York 11973, United States*

Rui Zu − *Department of Materials Science and Engineering, Pennsylvania State University, University Park, Pennsylvania 16802, United States;* orcid.org/0000-0002-9944-4757

Venkatraman Gopalan − *Department of Materials Science and Engineering, Department of Physics, and Department of Engineering Science and Mechanics, Pennsylvania State University, University Park, Pennsylvania 16802, United States;* orcid.org/0000-0001-6866-3677

Saul H. Lapidus − *Advanced Photon Source, Argonne National Laboratory, Lemont, Illinois 60439, United States;* orcid.org/0000-0002-7486-4325

Corey E. Frank − *Department of Chemistry and Chemical Biology, Rutgers, The State University of New Jersey, Piscataway, New Jersey 08854, United States*

Youguo Shi − *Beijing National Laboratory for Condensed Matter Physics, and Institute of Physics, Chinese Academy of Sciences, Beijing 100190, China*

David Walker − *Lamont Doherty Earth Observatory, Columbia University, New York 10964, United States*

Complete contact information is available at: https://pubs.acs.org/10.1021/acs.chemmater.1c02046

Author Contributions

#HLF and CJK contributed equally to this work.

Notes

The authors declare no competing financial interest.

■ ACKNOWLEDGMENTS

M.G. was supported by the Center for Computational Design of Functional Strongly Correlated Materials and Theoretical Spectroscopy under DOE grant no. DE-FOA-0001276. Work at Brookhaven National Laboratory was supported by the DOE BES (DE-SC0012704) on the NSLS-II Beamlines 8-ID and 7-BM and NSLS-I Beamline X19A. C.J.K. was supported by NRF (NRF-2021R1F1A1063691) and the National Superconducting Center with supercomputing resources including technical support KSC-2021-CRE-0133. B.K. acknowledges support by NRF grant No. 2021R1C1C1007017. K.K. was supported by the Internal R&D program at KAERI (No. 524460-21). R.Z. and V.G. acknowledge support from the NSF MRSEC Center for Nanoscale Science, DMR-2011839. Use of the Advanced Photon Source at Argonne National Laboratory was supported by the DOE, Office of Science, Office of Basic Energy Sciences, under contract no. DE-AC02-06CH11357.

■ REFERENCES

(1) Spaldin, N. A.; Ramesh, R. Advances in Magnetoelectric Multiferroics. *Nat. Mater.* **2019**, *18*, 203−212.

(2) Fiebig, M.; Lottermoser, T.; Meier, D.; Trassin, M. The Evolution of Multiferroics. *Nat. Rev. Mater.* **2016**, *1*, 16046.

(3) Cheong, S. W.; Mostovoy, M. Multiferroics: a Magnetic Twist for Ferroelectricity. *Nat. Mater.* **2007**, *6*, 13−20.

(4) Cai, G. H.; Greenblatt, M.; Li, M. R. Polar Magnets in Double Corundum Oxides. *Chem. Mater.* **2017**, *29*, 5447−5457.

(5) Li, M. R.; McCabe, E. E.; Stephens, P. W.; Croft, M.; Collins, L.; Kalinin, S. V.; Deng, Z.; Retuerto, M.; Sen Gupta, A.; Padmanabhan, H.; Gopalan, V.; Grams, C. P.; Hemberger, J.; Orlandi, F.; Manuel, P.; Li, W. M.; Jin, C. Q.; Walker, D.; Greenblatt, M. Magnetostriction-Polarization Coupling in Multiferroic Mn_2MnWO_6. *Nat. Commun.* **2017**, *8*, 2037.

(6) Hudl, M.; Mathieu, R.; Ivanov, S. A.; Weil, M.; Carolus, V.; Lottermoser, T.; Fiebig, M.; Tokunaga, Y.; Taguchi, Y.; Tokura, Y.; Nordblad, P. Complex Magnetism and Magnetic-Field-Driven Electrical Polarization of Co_3TeO_6. *Phys. Rev. B* **2011**, *84*, No. 180404.

(7) Kim, J. W.; Artyukhin, S.; Mun, E. D.; Jaime, M.; Harrison, N.; Hansen, A.; Yang, J. J.; Oh, Y. S.; Vanderbilt, D.; Zapf, V. S.; Cheong, S. W. Successive Magnetic-Field-Induced Transitions and Colossal Magnetoelectric Effect in Ni_3TeO_6. *Phys. Rev. Lett.* **2015**, *115*, No. 137201.

(8) Li, W. H.; Wang, C. W.; Hsu, D.; Lee, C. H.; Wu, C. M.; Chou, C. C.; Yang, H. D.; Zhao, Y.; Chang, S.; Lynn, J. W.; Berger, H. Interplay Between the Magnetic and Electric Degrees of Freedom in Multiferroic Co_3TeO_6. *Phys. Rev. B* **2012**, *85*, No. 094431.

(9) Skiadopoulou, S.; Borodavka, F.; Kadlec, C.; Kadlec, F.; Retuerto, M.; Deng, Z.; Greenblatt, M.; Kamba, S. Magnetoelectric Excitations in Multiferroic Ni_3TeO_6. *Phys. Rev. B* **2017**, *95*, No. 184435.

(10) Toledano, P.; Carolus, V.; Hudl, M.; Lottermoser, T.; Khalyavin, D. D.; Ivanov, S. A.; Fiebig, M. First-Order Multi-k Phase Transitions and Magnetoelectric Effects in Multiferroic Co_3TeO_6. *Phys. Rev. B* **2012**, *85*, No. 214439.

(11) Yokosuk, M. O.; Al-Wahish, A.; Artyukhin, S.; O'Neal, K. R.; Mazumdar, D.; Chen, P.; Yang, J.; Oh, Y. S.; McGill, S. A.; Haule, K.; Cheong, S. W.; Vanderbilt, D.; Musfeldt, J. L. Magnetoelectric Coupling Through the Spin Flop Transition in Ni_3TeO_6. *Phys. Rev. Lett.* **2016**, *117*, No. 147402.

(12) Yokosuk, M. O.; Artyukhin, S.; Al-Wahish, A.; Wang, X. Y.; Yang, J.; Li, Z. Q.; Cheong, S. W.; Vanderbilt, D.; Musfeldt, J. L. Tracking the Continuous Spin-Flop Transition in Ni_3TeO_6 by Infrared Spectroscopy. *Phys. Rev. B* **2015**, *92*, No. 144305.

(13) Li, M. R.; Croft, M.; Stephens, P. W.; Ye, M.; Vanderbilt, D.; Retuerto, M.; Deng, Z.; Grams, C. P.; Hemberger, J.; Hadermann, J.; Li, W. M.; Jin, C. Q.; Saouma, F. O.; Jang, J. I.; Akamatsu, H.; Gopalan, V.; Walker, D.; Greenblatt, M. Mn_2FeWO_6: A New Ni_3TeO_6-Type Polar and Magnetic Oxide. *Adv. Mater.* **2015**, *27*, 2177−2181.

(14) Li, M. R.; Walker, D.; Retuerto, M.; Sarkar, T.; Hadermann, J.; Stephens, P. W.; Croft, M.; Ignatov, A.; Grams, C. P.; Hemberger, J.; Nowik, I.; Halasyamani, P. S.; Tran, T. T.; Mukherjee, S.; Dasgupta, T. S.; Greenblatt, M. Polar and Magnetic Mn_2FeMO_6 (M=Nb, Ta) with $LiNbO_3$-type Structure: High-Pressure Synthesis. *Angew. Chem., Int. Ed.* **2013**, *52*, 8406−8410.

(15) Solana-Madruga, E.; Dos Santos-Garcia, A. J.; Arevalo-Lopez, A. M.; Avila-Brande, D.; Ritter, C.; Attfield, J. P.; Saez-Puche, R. High Pressure Synthesis of Polar and Non-Polar Cation-Ordered Polymorphs of Mn_2ScSbO_6. *Dalton Trans.* **2015**, *44*, 20441−20448.

(16) Ivanov, S. A.; Mathieu, R.; Nordblad, P.; Tellgren, R.; Ritter, C.; Politova, E.; Kaleva, G.; Mosunov, A.; Stefanovich, S.; Weil, M. Spin and Dipole Ordering in Ni_2InSbO_6 and Ni_2ScSbO_6 with Corundum-Related Structure. *Chem. Mater.* **2013**, *25*, 935−945.

(17) Mathieu, R.; Ivanov, S. A.; Bazuev, G. V.; Hudl, M.; Lazor, P.; Solovyev, I. V.; Nordblad, P. Magnetic Order Near 270 K in Mineral and Synthetic Mn_2FeSbO_6 ilmenite. *Appl. Phys. Lett.* **2011**, *98*, 202505.

(18) Feng, H. L.; Deng, Z.; Croft, M.; Lapidus, S. H.; Zu, R.; Gopalan, V.; Grams, C. P.; Hemberger, J.; Liu, S.; Tyson, T. A.; Frank, C. E.; Jin, C. Q.; Walker, D.; Greenblatt, M. High-Pressure Synthesis and Ferrimagnetism of Ni_3TeO_6-Type Mn_2ScMO_6 (M = Nb, Ta). *Inorg. Chem.* **2019**, *58*, 15953−15961.

(19) Zhao, L.; Hu, Z. W.; Kuo, C. Y.; Pi, T. W.; Wu, M. K.; Tjeng, L. H.; Komarek, A. C. Mn_3TeO_6 - A New Multiferroic Material with Two Magnetic Substructures. *Phys. Status Solidi RRL* **2015**, *9*, 730−734.

(20) Rodríguez-Carvajal, J.; Hennion, M.; Moussa, F.; Moudden, A. H.; Pinsard, L.; Revcolevschi, A. Neutron-Diffraction Study of the Jahn-Teller Transition in Stoichiometric $LaMnO_3$. *Phys. Rev. B* **1998**, *57*, R3189−R3192.

(21) Murakami, Y.; Hill, J. P.; Gibbs, D.; Blume, M.; Koyama, I.; Tanaka, M.; Kawata, H.; Arima, T.; Tokura, Y.; Hirota, K.; Endoh, Y. Resonant X-Ray Scattering From Orbital Ordering in $LaMnO_3$. *Phys. Rev. Lett.* **1998**, *81*, 582−585.
(22) Solovyev, I.; Hamada, N.; Terakura, K. Crucial Role of the Lattice Distortion in the Magnetism of $LaMnO_3$. *Phys. Rev. Lett.* **1996**, *76*, 4825−4828.
(23) Mizokawa, T.; Khomskii, D. I.; Sawatzky, G. A. Interplay Between Orbital Ordering and Lattice Distortions in $LaMnO_3$, YVO_3, and $YTiO_3$. *Phys. Rev. B* **1999**, *60*, 7309−7313.
(24) Feng, H. L.; Ghimire, M. P.; Hu, Z. W.; Liao, S.-C.; Agrestini, S.; Chen, J.; Yuan, Y.; Matsushita, Y.; Tsujimoto, Y.; Katsuya, Y.; Tanaka, M.; Lin, H.-J.; Chen, C.-T.; Weng, S.-C.; Valvidares, M.; Chen, K.; Baudelet, F.; Tanaka, A.; Greenblatt, M.; Tjeng, L. H.; Yamaura, K. Room-Temperature Ferrimagnetism of Anti-Site-Disordered Ca_2MnOsO_6. *Phys. Rev. Mater.* **2019**, *3*, No. 124404.
(25) Walker, D.; Carpenter, M. A.; Hitch, C. M. Some Simplifications to Multianvil Devices for High-Pressure Experiments. *Am. Mineral.* **1990**, *75*, 1020−1028.
(26) Denev, S. A.; Lummen, T. T. A.; Barnes, E.; Kumar, A.; Gopalan, V. Probing Ferroelectrics Using Optical Second Harmonic Generation. *J. Am. Ceram. Soc.* **2011**, *94*, 2699−2727.
(27) Sen Gupta, A.; Akamatsu, H.; Brown, F. G.; Nguyen, M. A. T.; Strayer, M. E.; Lapidus, S.; Yoshida, S.; Fujita, K.; Tanaka, K.; Tanaka, I.; Mallouk, T. E.; Gopalan, V. Competing Structural Instabilities in the Ruddlesden Popper Derivatives $HRTiO_4$ (R = Rare Earths): Oxygen Octahedral Rotations Inducing Noncentrosymmetricity and Layer Sliding Retaining Centrosymmetricity. *Chem. Mater.* **2017**, *29*, 656−665.
(28) Sen Gupta, A.; Akamatsu, H.; Strayer, M. E.; Lei, S. M.; Kuge, T.; Fujita, K.; Dela Cruz, C.; Togo, A.; Tanaka, I.; Tanaka, K.; Mallouk, T. E.; Gopalan, V. Improper Inversion Symmetry Breaking and Piezoelectricity through Oxygen Octahedral Rotations in Layered Perovskite Family, $LiRTiO_4$ (R = Rare Earths). *Adv. Electron. Mater.* **2016**, *2*, No. 1500196.
(29) Garten, L. M.; Burch, M.; Gupta, A. S.; Haislmaier, R.; Gopalan, V.; Dickey, E. C.; Trolier-McKinstry, S. Relaxor Ferroelectric Behavior in Barium Strontium Titanate. *J. Am. Ceram. Soc.* **2016**, *99*, 1645−1650.
(30) Strayer, M. E.; Sen Gupta, A.; Akamatsu, H.; Lei, S. M.; Benedek, N. A.; Gopalan, V.; Mallouk, T. E. Emergent Noncentrosymmetry and Piezoelectricity Driven by Oxygen Octahedral Rotations in n=2 Dion-Jacobson Phase Layer Perovskites. *Adv. Funct. Mater.* **2016**, *26*, 1930−1937.
(31) Izumi, F.; Ikeda, T. A Rietveld-Analysis Programm RIETAN-98 and Its Applications to Zeolite. *Mater. Sci. Forum* **2000**, *321-324*, 198−205.
(32) Izumi, F.; Momma, K. Three-Dimensional Visualization in Powder Diffraction. *Solid State Phenom.* **2007**, *130*, 15−20.
(33) Croft, M.; Sills, D.; Greenblatt, M.; Lee, C.; Cheong, S. W.; Ramanujachary, K. V.; Tran, D. Systematic Mn D-configuration Change in the $La_{1-x}Ca_xMnO_3$ System: A Mn K-edge SAS study. *Phys. Rev. B* **1997**, *55*, 8726−8732.
(34) Mandal, T.; Abakumov, A.; Lovanov, M.; Poltavets, V.; Croft, M.; Stalick, J.; Greenblatt, M. Synthesis, Structure and Magnetic Properties of $SrLaMnSbO_6$: A New B-site Ordered Double Perovskite. *Chem. Mater.* **2008**, *20*, 4653−4660.
(35) Mandal, T. K.; Croft, M.; Hadermann, J.; Van Tendeloo, G.; Stephens, P. W.; Greenblatt, M. La_2MnVO_6 Double Perovskite: A Structural, Magnetic and X-Ray Absorption Investigation. *J. Mater. Chem.* **2009**, *19*, 4382−4390.
(36) Lin, Q.; Greenblatt, M.; Croft, M. Evolution of Structure and Magnetic Properties in Electron-Doped Double Perovskites, $Sr_{2-x}La_xMnWO_6$ (0<x<1). *J. Solid State Chem.* **2005**, *178*, 1356−1366.
(37) Blaha, P.; Schwarz, K.; Tran, F.; Laskowski, R.; Madsen, G. K. H.; Marks, L. D. WIEN2k: An APW+lo Program for Calculating the Properties of Solids. *J. Chem. Phys.* **2020**, *152*, No. 074101.
(38) Perdew, J. P.; Burke, K.; Ernzerhof, M. Generalized Gradient Approximation Made Simple. *Phys. Rev. Lett.* **1996**, *77*, 3865.
(39) Anisimov, V. I.; Solovyev, I. V.; Korotin, M. A.; Czyzyk, M. T.; Sawatzky, G. A. Density-Functional Theory and NiO Photoemission Spectra. *Phys. Rev. B* **1993**, *48*, 16929.
(40) Anisimov, V. I.; Aryasetiawan, F.; Lichtenstein, A. I. First-Principle Calculations of the Electronic Structure and Spectra of Strongly Correlated Systems: the LDA + U Method. *J. Phys.: Condens. Matter* **1997**, *9*, 767.
(41) Zivkovic, I.; Prsa, K.; Zaharko, O.; Berger, H. Ni_3TeO_6-A Collinear Antiferromagnet with Ferromagnetic Honeycomb Planes. *J. Phys.: Condens. Matter* **2010**, *22*, No. 056002.
(42) Floris, A.; de Gironcoli, S.; Gross, E. K. U.; Cococcioni, M. Vibrational properties of MnO and NiO from DFT+U-based density functional perturbation theory. *Phys. Rev. B* **2011**, *84*, No. 161102(R).
(43) Feng, H. L.; Yamaura, K.; Tjeng, L. H.; Jansen, M. The Role of Nonmagnetic d^0 vs. d^{10} B-Type Cations on the Magnetic Exchange Interactions in Osmium Double Perovskites. *J. Sold State Chem.* **2016**, *243*, 119−123.
(44) Kanungo, S.; Yan, B.; Felser, C.; Jansen, M. Active Role of Nonmagnetic Cations in Magnetic Interactions for Double-Perovskite Sr_2BOsO_6 (B = Y, In, Sc). *Phys. Rev. B* **2016**, *93*, No. 161116(R).

https://doi.org/10.1021/acs.chemmater.1c02046
Chem. Mater. 2021, 33, 6522−6529